Novel low-ε_r and lightweight $LiBO_2$ microwave dielectric ceramics with good chemical compatibility with silver

Changzhi Yin[1], Kang Du[1], Meng Zhang[1], Jiaqing Yang[1], Fei Wang[1], Yanbo Guo[1], Mingfei Cheng[1], Yiyang Cai[1], Xiaoqiang Song[3], Jibran Khaliq[5], Chunchun Li[4*], Wen Lei[1,2,3*], Wenzhong Lu[1,2,3]

[1]*School of Optical and Electronic Information, Key Lab of Functional Materials for Electronic Information (B) of MOE, Huazhong University of Science and Technology, Wuhan, P. R. China*

[2]*Wuhan National Laboratory for Optoelectronics, Huazhong University of Science and Technology, Wuhan, P. R. China*

[3]*Wenzhou Advanced Manufacturing Institute, Huazhong University of Science and Technology, Wenzhou, P. R. Ch*

[4]*College of Material Science and Engineering, Guilin University of Technology, Guilin 541004, China*

[5]*Department of Mechanical and Construction Engineering, Faculty of Engineering and Environment, Northumbria University at Newcastle, Newcastle upon Tyne NE1 8ST, U.K.*

Abstract

High-speed signal propagation systems require dielectric ceramics with low relative permittivity (ε_r) and a high-quality factor (Qxf). In this paper, a novel low-permittivity borate ceramic ($LiBO_2$) was synthesized using a conventional solid-state reaction method. Based on the X-ray diffraction and Rietveld refinement, the $LiBO_2$ crystallized into a monoclinic structure with a space group of P21/c. Dense and single-phase ceramic was obtained at 640 °C with comprehensive microwave dielectric properties: a low relative permittivity (ε_r) of 5.3, a moderate quality factor ($Q\times f$) of 18,200 GHz at 16.3 GHz, and a temperature coefficient of resonant frequency (τ_f) of -66.2 ppm/°C. Good chemical compatibility with Ag electrode and thermal expansion coefficient of 25.4 ppm/°C was achieved demonstrating the potential applications as dielectric resonances in wireless communications and substrates in low-temperature cofired ceramics.

Keywords: Ceramics; Dielectric properties; Wireless communication; low-permittivity

* Authors to whom correspondence should be addressed: lichunchun2003@126.com (C.C. Li), wenlei@mail.hust.edu.cn (W. Lei).

Introduction

The rapid growth of wireless communication has driven the demand for microwave dielectric ceramics (MDCs) with suitable dielectric properties, such as acceptable dielectric permittivity (ε_r), high quality factor (*Qxf*), and near-zero temperature coefficient of resonant frequency (τ_f). [1-4]. These materials have been successfully commercialized in a fifth-generation cellular wireless system (5G) and possess prominent features (high speed, high capacity, low latency, etc.). The frequency bands in 5G technology have been extended to the millimeter-wave range (~ 39 GHz), which is still in its infancy as it covers very short ranges and is currently expensive to implement [5, 6].

For 5G technology, low latency is a key feature and one of the most significant merits of its processes. The source of latency is the delay time (t_d), which indicates signal propagation in dielectric materials. The delay time is given by the equation $t_d = \sqrt{\varepsilon_r} l_e / c$ (where l_e is the transmission distance, and *c* is the velocity of light), the signal delay time is directly proportional to the square root of relative permittivity [7-9]. As a result, the low ε_r materials are desirable to reduce signal delay. Although high relative permittivity is favorable for device miniaturization, however, with a shift to a higher frequency, the aspiration of miniaturization is less significant compared to the signal delay.

The relative permittivity can be estimated by the Clausius-Mosotti equation $\varepsilon_r = (3V + 8\pi\alpha)/(3V - 4\pi\alpha)$, where α is molecular polarizability, and *V* is cell volume [10-12]. As can be seen, the relative permittivity is directly proportional to ionic polarizability per cell volume which gives research directions to explore the low-permittivity ceramics with low polarizability (such as silicates, aluminates, and borates) [13-16]. Furthermore, to achieve miniaturization and rapid synthesis of ceramics, the low temperature co-fired ceramics (LTCC) are often employed, which has an added advantage of simultaneously processing the dielectrics and conductive electrode materials (such as Al, Ag, and Cu) [2]. For low-temperature co-firing, one of the requirements is that the sintering and densification temperature of these dielectrics

should be below the melting point of electrode materials (e.g., 660 °C for Al, 960 °C for Ag, and 1060 °C for Cu) [2]. Despite the fact that a large number of dielectrics with low dielectric loss have been synthesized in recent decades, the majority of them have been densified at rather high temperatures. (>1000 °C). Thus, the ongoing challenge in the LTCC technology is to design materials meeting the strict requirements.

Recently, researchers have focused on the borates since the B^{3+} has extremely low polarizability of 0.05 Å and B_2O_3 has a low melt point of 450 °C [10]. Bian *et al.* reported that the $LiCaBO_3$ and $LiSrBO_3$ ceramics have excellent microwave dielectric properties sintered at 800 °C: ε_r = 8.7 and 8.6, $Q \times f$ = 75,000 and 60,000 GHz, τ_f = -150 and -39 ppm/°C, respectively [17]. Li *et al.* reported that the $LiBGeO_4$ ceramic sintered at 820 °C has a low relative permittivity of 6.28 [18]. Zhou et al. have synthesized $Li_6B_4O_9$ ceramics at 640 °C with ε_r = 5.95 which also has good chemical compatibility with silver electrodes [19].

$LiBO_2$ crystallizes in monoclinic α-phase and tetragonal γ-phase depending on preparation conditions [20]. The presence (α-phase) or absence (γ-phase) of a center of symmetry is the main difference between the two structures. As a result, the short-range order is present in the crystal due to the symmetry of the α-phase and is lower than the γ-phase but the unit volume is twice as the γ-phase. The crystal structure is mostly determined by the boron-oxygen groups. The $(BO_3)^{3-}$ trigonal groups elongate along the [010] direction and are interconnected through oxygen atoms. In turn, the infinite $[(BO_3)^{3-}]_n$ chains are interconnected by weak, predominantly ionic, Li-O bonds. The strong interaction along the b-axis and low interaction along the *a*- and *c*- axis caused the high physical properties of anisotropy.

In this paper, new low-ε_r microwave dielectric ceramics, $LiBO_2$ ceramics were synthesized by a conventional solid-state method. The phase composition, crystal structure, microstructure, and microwave dielectric properties were analyzed via X-ray diffraction, Rietveld refinement, Raman spectra, and packing fraction. The chemical stability and thermal expansion coefficient were also investigated.

Experimental procedure

The $LiBO_2$ ceramics were synthesized by a solid-state reaction method using reagent grade ceramic powders Li_2CO_3 and H_3BO_3 (99.99%, Aladdin Industrial Corporation). Stoichiometric starting powders were weighed and then ball-milled with zirconia balls as a grinding media and ethanol in a nylon jar for 6 h. 15 wt.% excess of H_3BO_3 was executed to make up for the loss of B_2O_3 during the pre-reaction process. Then, the slurries were dried at 80 °C, sieved with 40-mesh, and calcined at 500 °C for 6 h to synthesize the $LiBO_2$ phase. The calcined powders were re-milled for 6 h under the same condition as mentioned above. After drying, the powders were mixed with 5wt.% PVA, pressed into a cylinder with Φ10×6.5 mm under a pressure of 20 MPa. The cold-pressed specimens were initially calcined at 550 °C for 2 h to remove the organic binder and then sintered at 580-660 °C for 6 h.

The phase composition was determined using the X-ray diffraction method with CuKα radiation (X'Pert PRO). The Rietveld refinement was employed to analyze crystal structure and atom position. The Rietveld parameters of the scale factor, zero shift, unit cell parameters, background polynomial, profile parameters, atomic positional coordinates, and isothermal factors were step-by-step refined to improve the value of reliability factors. The thermal etched microstructures of $LiBO_2$ samples sintered at different temperatures were observed by scanning electron microscope (SEM; Quanta 200). The thermal etching was performed for 30 min at 80 °C below the sintering temperature. The density of all samples was measured via Archimede's method. The relative permittivity and dielectric loss were measured by a network

analyzer (Model N5230 A, Agilent Co, Palo Alto, California) in the TE_{011} mode with the Hakki and Coleman method [21]. The τ_f values were measured in the temperature range of T_1 (25 °C) to 85 °C T_2 and calculated based on the following equation:

$$\tau_f = \frac{f_2 - f_1}{f_1(T_2 - T_1)} \qquad (1)$$

Where f_1 and f_2 represent resonant frequency at 25 °C and 85 °C, respectively. The room-temperature infrared reflectivity spectra were measured by a Bruker IFS 66v FT-IR spectrometer (Bruker Optics, Ettlingen, Germany). The thermal expansion coefficient was measured with the NETZSCH DIL402C thermal expansion instrument.

Result and discussion

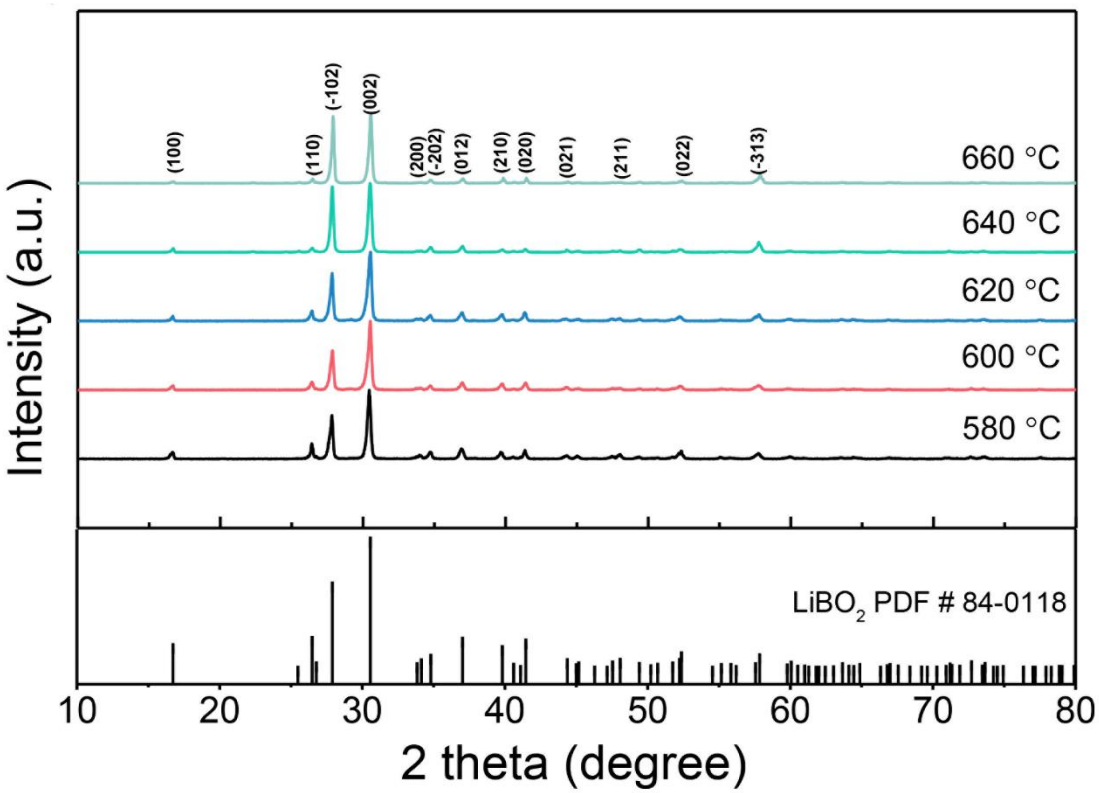

Figure 1 the X-ray patterns of $LiBO_2$ ceramics sintered at different temperatures

Figure 1 shows the X-ray diffraction patterns of $LiBO_2$ ceramics sintered at 580-660 °C for 6 h. All the peaks matched well with PDF # 84-0118 and no other peaks

were detected, indicating that the single phase of $LiBO_2$ with monoclinic structure (α phase) was obtained at a relatively wide temperature range.

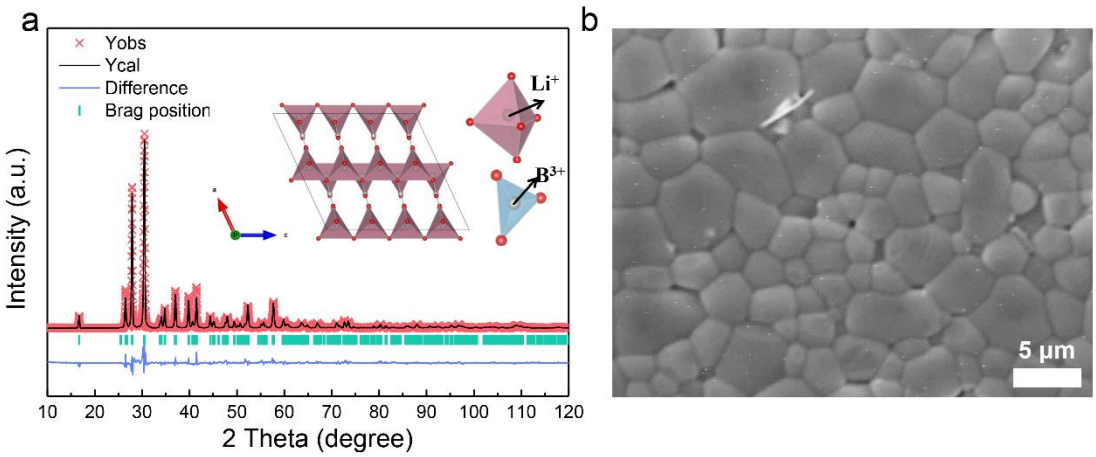

Figure 2 (a) Rietveld refinement pattern of $LiBO_2$ ceramic (the crystal structure of $LiBO_2$ along b direction is shown in inset), (b) the microstructure of $LiBO_2$ ceramic sintered at 640 °C.

To further investigate the phase composition and structure of $LiBO_2$ ceramic, Rietveld refinement using Fullprof software was carried out on the X-ray diffraction pattern measured on the - sample sintered at 640 °C. Table S1 shows the atoms positions, reliability factors, and reliability of fitness indicators of the refined result. As shown in Figure 2, a good match between measured and calculated data and low goodness of fit index (χ^2) indicated that the structure model is reliable for refinement. The lattice parameters were a = 5.8473(4) Å, b = 4.3548(1) Å, c = 6.4673(9) Å, and V = 149.38(9) $Å^3$. The inset of Figure 2a shows a structure sketch of $LiBO_2$ based on the refinement result. The $(BO_3)^{3-}$ groups elongate along the b-axis and are connected with Li atoms through oxygen atoms. Li^+ cations have a coordination number of 5 and form a hexahedron with oxygen. The thermally etched surface of $LiBO_2$ at 640 °C was shown in Figure 2b which reveals a dense microstructure with an average grain size in the range of 2-4 μm.

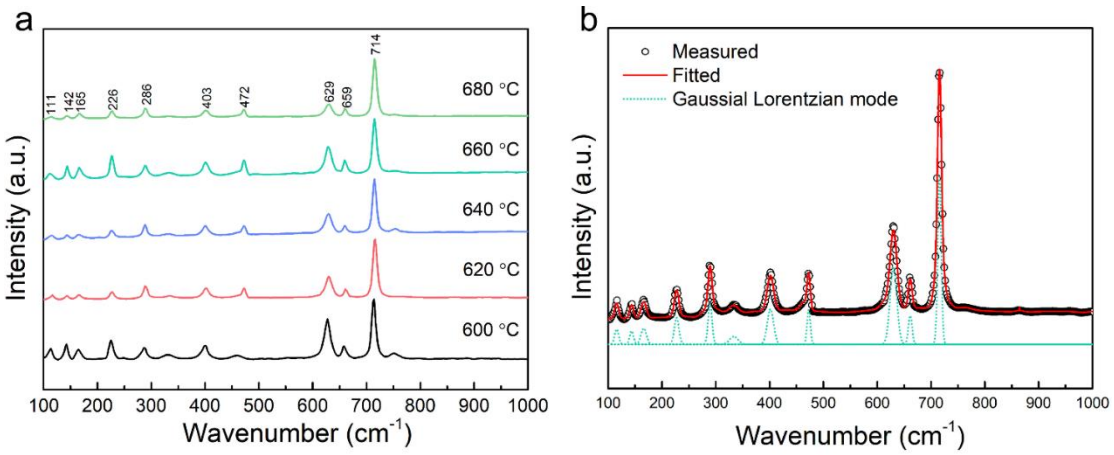

Figure 3 (a) Raman spectroscopy for $LiBO_2$ ceramic sintered at different temperatures; (b) the Gauss-Lorenzian deconvolution for $LiBO_2$ ceramic sintered at 640 °C.

Raman scattering is known to be sensitive to the local structure variation [22]. Typically, for a monoclinic structure with a P21/c space group, the active modes can be predicted based on the factor group correlation [22, 23]:

$$\Gamma = 9A_g + 9A_u + 9B_g + 9B_u \qquad (2)$$

Where the A_g and B_g represent the Raman active mode while the A_u and B_u are the IR active modes. As shown in Figure 3a, the Raman spectra of $LiBO_2$ ceramics sintered at different temperatures showed similar profiles which further indicated the temperature stability of $LiBO_2$ ceramics. Figure 3b shows the fitting result of $LiBO_2$ sintered at 660 °C via the Gauss-Lorenzian deconvolution. Due to the low intensity and overlapping of some modes, only 11 active Raman modes were observed. The strongest peak around 716 cm^{-1} was assigned to the vibration of the B-O-B bond bending. The peak at 490 cm^{-1} was related to the vibrations of the LiO_4 group, and the bond at 420 cm^{-1} is related to the vibrations of the Li-O bond in hexahedron [22].

As shown in Figure 4a, the density initially increased from 1.97 g/cm^3 (with relative density 90.2%) at 580°C to 2.07 g/cm^3 (95.1%) at 640 °C and then slightly decreased to 2.05 g/cm^3 (94.4%) at 660 °C. As a well-established fact, the microwave dielectric properties depend on the intrinsic factor (such as lattice vibration, packing fraction, etc.) and extrinsic factors (such as the second phase, density, grain size, phase transition, etc.) [24-27]. Keeping this in view, the influence of density and microstructure on the microwave dielectric properties will be analyzed below.

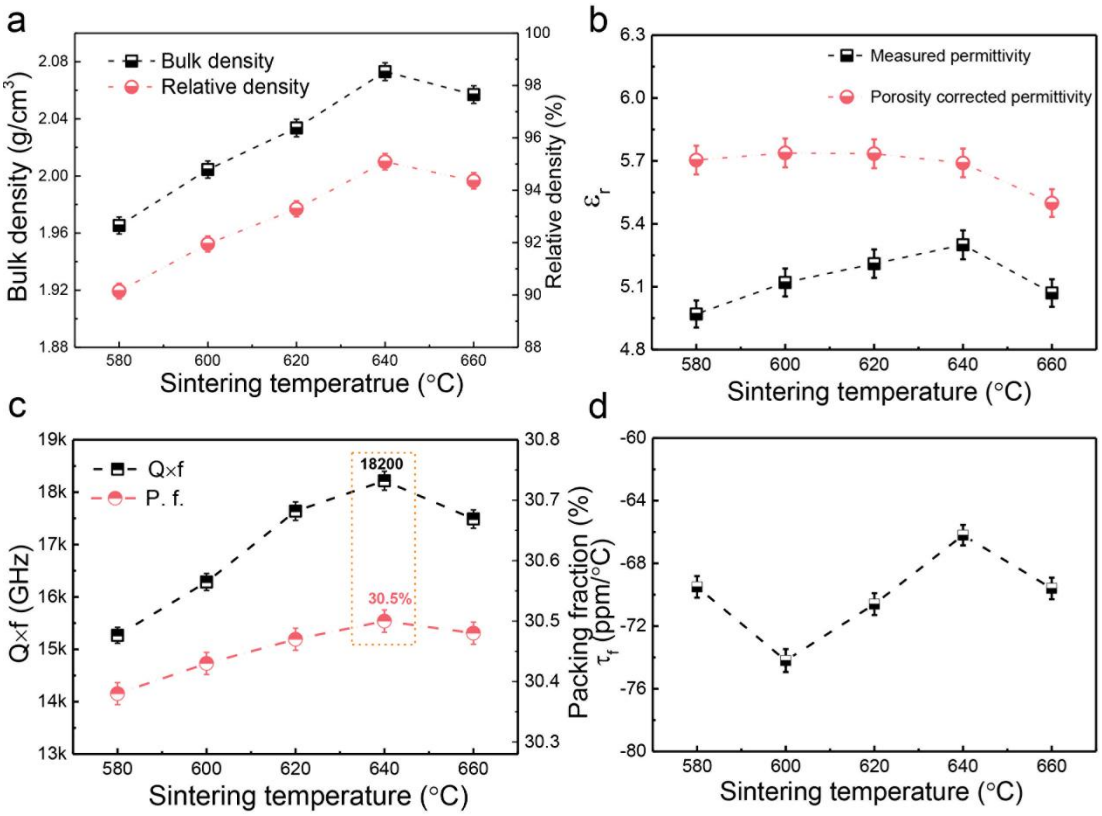

Figure 4 the density and microwave dielectric properties of $LiBO_2$ ceramic as a function of sintering temperature.

Figure 4b-d shows the dependence of (ε_r, $Q\times f$, and τ_f) on the varying sintering temperature. Both relative permittivity and quality factor showed similar variation tendency to density with increasing sintering temperature, indicating that density was a dominant factor affecting both relative permittivity and quality factor. The relative permittivity gradually increased initially from 4.97 at 580 °C to 5.3 at 640 °C and then slightly decreased to 5.07 with further increasing sintering temperature up to 660 °C. A similar variation was seen for the quality factor and the maximum value of 18,200 GHz was achieved at 640 °C. From the variation trend of microwave dielectric properties, the optimum microwave dielectric properties could be obtained at 640 °C. The relationship between relative permittivity and density could be explained by the fact that open porosity essentially contains air which has a relative permittivity value of ~1 much lower than the $LiBO_2$ ceramic. This means that ceramics with higher relative density would exhibit higher relative permittivity while a lower relative permittivity was a result of a lower relative density at 660 °C. To eliminate the influence of porosity on relative permittivity, the Bosman and Having's equation was employed [28-30]:

$$\varepsilon_{corr} = \varepsilon_r(1+1.5P) \qquad (3)$$

Where the P represents the fractional porosity. As shown in Figure 4b, the corrected permittivity values were slightly higher than the measured values and nearly matched the measured values with the increasing sintering temperature and the smallest difference (Δ = 7.4%) was obtained at 640 °C. Besides, it should be noted that the measured values were similar to the calculated ones based on the Clausius-Mossotti equation (ε_{theo} = 5.33) [10].

It is generally accepted that the microwave dielectric properties were determined by the extrinsic factor (e.g., grain size, pore, crystal defects, etc) and intrinsic factor (e.g., crystal structure, packing fraction, bond natures, etc) [6, 25]. Based on the X-ray diffraction and the Rietveld refinement, the influence of the secondary phase on microwave dielectric properties can be ruled out. The high packing fraction (P. F.) indicated the low interspace for lattice vibration with a low dielectric loss [31, 32]. As shown in Figure 4c, the packing fraction significantly increased with the sintering temperature increasing reaching a peak value of 30.5% at 640 °C, which suggested an improvement in the ion packing resulting in the dielectric loss decrease. Compared with other highly packed systems, such as $CaMoO_4$ (P. F. = 61.6%, $Q\times f$ = 76,990 GHz), $PbWO_4$ (P. F. = 56.8%, $Q\times f$ = 34,500 GHz), and $LaNbO_4$, (P. F. = 64.9%, $Q\times f$ = 50,700 GHz), a much lower packing fraction of $LiBO_2$ may be one of the origins of its lower quality factor [31].

On the contrary, the τ_f values obtained were between -66.2 and -74.2 ppm/°C, exhibiting a weak dependence on sintering temperature since no second phase or phase transition emerged over the temperature range. To regulate the τ_f values to near zero, researchers have primarily used two strategies. The first way is to combine certain materials with positive τ_f values, such as TiO_2 (τ_f = +450 ppm/°C) and $CaTiO_3$ (τ_f = +800 ppm/°C) to make composite ceramics. The second strategy is to tune the τ_f values to near zero by forming a solid solution through doping or substitution. In this work, we have employed $CaTiO_3$ to adjust the negative τ_f values of $LiBO_2$ ceramic. As shown in Figure S1, the $LiBO_2$ ceramic has a chemical reaction with $CaTiO_3$ ceramic to form

Li_2TiO_3 and another unknown phase.

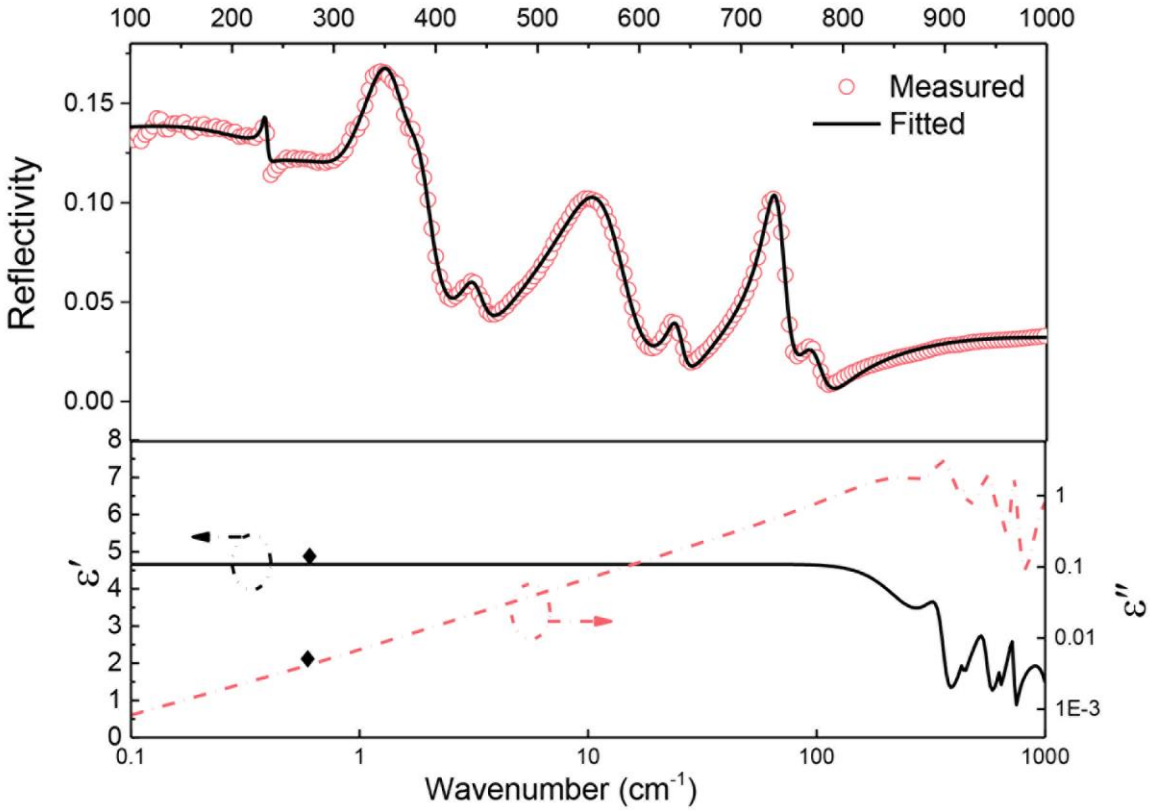

Figure 5 Measured and calculated far-infrared reflectivity spectra and fitted complex dielectric spectra of $LiBO_2$ ceramic sintered at 640 °C

To estimate the intrinsic microwave dielectric characteristics, the Kramers-Kronig (K-K) approach was frequently used to fit the far-infrared reflectance spectrum. Figure 5 shows the IR spectrum of $LiBO_2$ ceramic sintered at 640 °C in which the contributions of lattice vibration on the microwave dielectric properties were extrapolated by fitting the IR reflectivity spectrum. The dielectric constant is mainly derived from the ionic and electronic displacement polarization at microwave bands [33, 34]. For dielectric loss, the extrapolated values were generally considered as the intrinsic dielectric loss. The measured spectrum was fitted based on a classical harmonic oscillator which was defined as follows:

$$R(\omega) = \left| \frac{\sqrt{\varepsilon^*(\omega)} - 1}{\sqrt{\varepsilon^*(\omega)} + 1} \right|^2 \qquad (4)$$

$$\varepsilon^*(\omega) = \varepsilon'(\omega) - i\varepsilon''(\omega)$$
$$= \varepsilon_\infty + \sum_{j=1}^{n} \frac{S_j(\omega_j^2 - \omega^2)}{(\omega_j^2 - \omega^2)^2 + \omega^2\gamma^2} - i\sum_{j=1}^{n} \frac{S_j\omega\gamma_j}{(\omega_j^2 - \omega^2)^2 + \omega^2\gamma^2} \quad (5)$$

where n represents the order of transverse polar-phonon modes; ω_j, S_j, and j_γ denote the frequency, strength, and damping constant of the j-th mode; and ε_∞ is the high-frequency relative permittivity induced by electronic polarization. Furthermore, the equations 4 and 5 can evolve to equations 6-8 at the conditions of $\omega << \omega_j$:

$$\varepsilon'(\omega) = \varepsilon_\infty + \sum_{j=1}^{n} \Delta\varepsilon_j' = \varepsilon_\infty + \sum_{j=1}^{n} \frac{\omega_{pj}}{\omega_{oj}^2} \quad (6)$$

$$\varepsilon''(\omega) \approx \sum_{j=1}^{n} \frac{\omega_{pj}^2\gamma_j}{\omega_{oj}^2}\omega \quad (7)$$

$$\tan\delta = \frac{\varepsilon''}{\varepsilon'} = \sum_{j=1}^{n} \frac{S_j\omega\gamma_j}{\varepsilon'(\omega)\omega_j^4} \quad (8)$$

As shown in Figure 5, there are 7 modes obtained for $LiBO_2$ ceramic, and phonon vibrations are shown in Table S2. These modes at 66.42 cm^{-1}, 260.9 cm^{-1}, 352.89 cm^{-1}, and 561.46 cm^{-1} are major contributors for the dielectric characteristics. Based on the real and imaginary parts of the complex permittivity, the calculated permittivity was 4.98 (ε_∞ = 1.51) at the microwave range in close agreement with the measured permittivity (ε_{mea} = 5.3). The theoretical quality factor had a value of 19,900 GHz which was also in agreement with the measured value. These results indicate that the contributions to polarization mainly concentrate on the absorption of structural phonon oscillation rather than the defect phonon scattering.

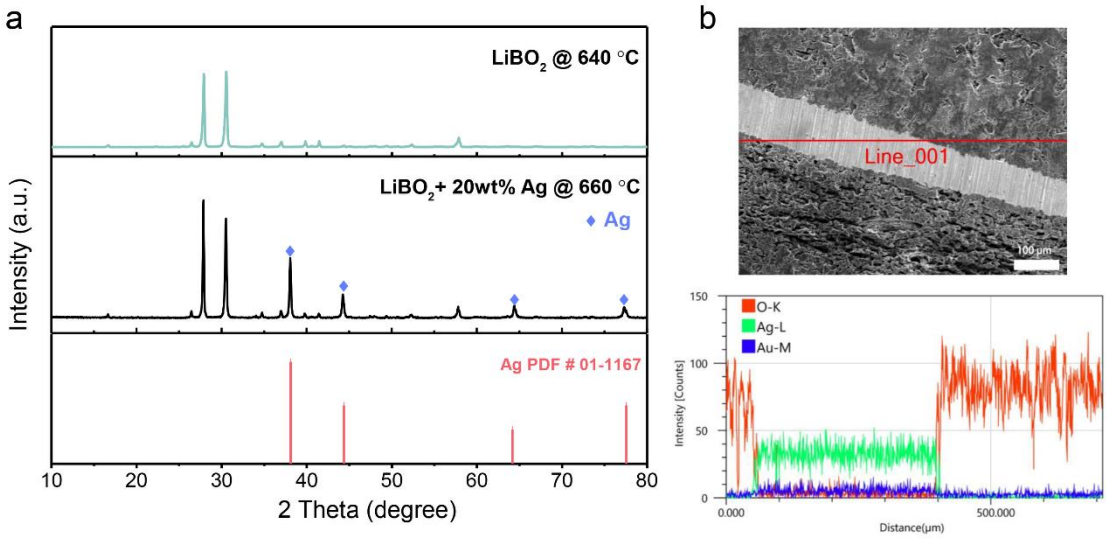

Figure 6 (a) the XRD patterns for $LiBO_2$ ceramic co-fired with Ag electrode; (b) the fractured surface after polished of $LiBO_2$ ceramic co-fired with Ag electrode and the EDS analysis of the selected line.

Due to the lower densification temperature of $LiBO_2$ compared to the Ag (melting point = 961 °C), it has the potential to be used in LTCC technology with no chemical reaction with the Ag electrode. Figure 6a describes the XRD patterns of $LiBO_2$ co-fired with 20 wt.% Ag powders at 640 °C. Only the diffraction peaks belonging to $LiBO_2$ and Ag could be detected depicting the lack of reaction between $LiBO_2$ and Ag. Figure 6b shows the SEM micrograph of the fractured surface of composite ceramics and EDS analysis of the selected line for the co-fired ceramic. a clear dense boundary between $LiBO_2$ ceramic and Ag electrode could be seen which further demonstrates the lack of reaction between $LiBO_2$ and Ag. EDS analysis indicates clear element distribution for different areas suggesting that the $LiBO_2$ ceramic has good chemical compatibility with the Ag electrode which makes $LiBO_2$ a potential candidate for LTCC technology. Figure S2 shows the XRD pattern of co-fired $LiBO_2$ with 20 wt.% Al at 640 °C for 30 min. In addition to the diffraction peaks of $LiBO_2$ (PDF # 84-0118) and Al (PDF # 01-1176), some extra peaks from an unknown phase were also detected which indicates that the $LiBO_2$ ceramic has a chemical reaction with the Al electrode.

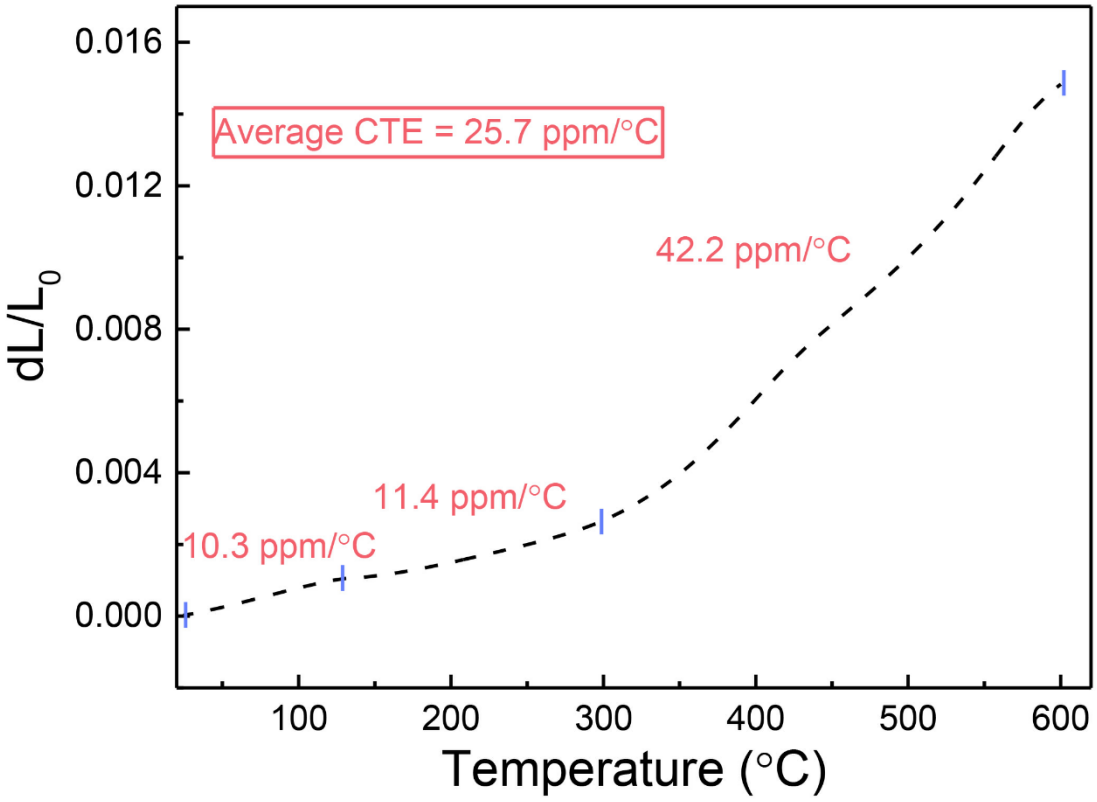

Figure 7 the thermal expansion coefficient of $LiBO_2$ ceramic measured at 25-600 °C.

To utilize LTCC technology, the thermal expansion coefficient match between the ceramics and metal electrodes is crucial. Figure 7 shows the thermal expansion of $LiBO_2$ ceramic as a function of temperature (between room temperature to 600 °C), from which the thermal expansion coefficient (α_L) was calculated. As shown in Figure 7, the $LiBO_2$ ceramic has a low α_L ~ 10 ppm/°C between room temperature to 300 °C. However, upon further increasing the temperature, α_L jumps to a much larger value ~ 42.2 ppm/°C in the temperature range of 300 °C to 600 °C. within the entire temperature range, the average thermal expansion coefficient was 25.4 ppm/°C, similar to the Ag (19 ppm/°C) and Al (23.6 ppm/°C) electrode, indicating that the $LiBO_2$ ceramic is a potential candidate for LTCC technology.

Table 1 The microwave dielectric properties and densification temperature of some borate ceramics

Compound	S.T. (°C)	ε_r	$Q\times f$ (GHz)	τ_f (ppm/°C)	Reference
$Li_6B_4O_9$	640	5.95	41,800	-72	[19]

$LiBGeO_4$	820	6.28	21,620	-88.7	[18]
$Bi_6B_{10}O_{24}$	660	10	10,800	-41	[35]
$Bi_4B_2O_9$	625	39	2600	-203	[35]
$BaCu(B_2O_5)$	810	7.4	50,000	-32	[36]
$Li_3AlB_2O_6$	640	6.0	41,800	-72	[37]
$Mg_3B_2O_6$	1300	7.2	230,900	-42	[38]
$Mg_2B_2O_5$	1280	6.2	32,100	-18	[38]
$Zn_3B_2O_6$	925	6.7	58,500	-58	[16]
$LiBO_2$	640	5.3	18,200	-66.2	This work

Table 1 compares microwave dielectric properties and densification temperature of borate ceramics. Generally, borates show promising microwave dielectric properties and low densification temperature, properties required for their potential utilization in LTCC technology. By comparison, most candidates with alkali metals or alkaline earth elements have low permittivities (ε_r < 7) whereas those Bi-containing compounds possess relatively higher permittivities (e.g., $Bi_4B_2O_9$ with ε_r ~ 39). However, the present $LiBO_2$ ceramic has an ultralow densification temperature (640 °C) and a low relative permittivity (ε_r ~ 5.3) which indicates the enormous potential in the LTCC field for this particular ceramic. however, their non-zero τ_f values should be suppressed to guarantee their commercial promotion.

Conclusions

A novel borate $LiBO_2$ ceramic with low permittivity and sintering temperature has been synthesized by the conventional solid-state method. Based on the X-ray diffraction and Rietveld refinement result, the $LiBO_2$ crystallized into a monoclinic structure (α-phase) with space group P21/c. Dense ceramic was obtained at a sintering temperature of 640 °C for 6 h with excellent comprehensive microwave dielectric properties: a low relative permittivity (ε_r) of 5.3, a moderate quality factor ($Q \times f$) of 18,200 GHz, and a temperature coefficient of resonant frequency (τ_f) of -66.2 ppm/°C. Good chemical

compatibility with Ag electrode and suitable thermal expansion coefficient (~25.4 ppm/°C) have been obtained. All results demonstrate the potential applications of $LiBO_2$ ceramic as dielectric resonators in wireless communications and substrates in low-temperature cofired ceramics.

ACKNOWLEDGMENTS

This work was supported by the National Natural Science Foundation of China (NSFC- 52072133 and 62061011) and the Innovation Team Program of Hubei Province, China (2019CFA004). The authors are grateful to the Analytical and Testing Center, Huazhong University of Science and Technology, for SEM analyses. The authors would also like to thank the administrators in the IR beamline workstation of the National Synchrotron Radiation Laboratory (NSRL) for their help in the IR measurement.

References

[1] M.T. Sebastian, Dielectric materials for wireless communication, Elsevier Publishers, Oxford, U.K., 2008.

[2] M.T. Sebastian, H. Jantunen, Low loss dielectric materials for LTCC applications: a review, Int. Mater. Rev. 53 (2008) 57-90.

[3] H.F. Zhou, J.Z. Gong, N. Wang, X.L. Chen, A novel temperature stable microwave dielectric ceramic with low sintering temperature and high quality factor, Ceram. Int. 42 (2016) 8822-8825.

[4] Y.K. Yang, H.L. Pan, H.T. Wu, Sintering characteristics and microwave dielectric properties of $Li_2Mg_3Ti_{0.95}(Mg_{1/3}Sb_{2/3})_{0.05}O_6$ ceramic doped with LiF for LTCC applications, J. Electron. Mater. 48 (2019) 2712-2717.

[5] D. Zhou, L.X. Pang, D.W. Wang, C. Li, B.B. Jin, I.M. Reaney, High permittivity and low loss microwave dielectrics suitable for 5G resonators and low temperature co-fired ceramic architecture, J. Mater. Chem. C 5 (2017) 10094-10098.

[6] Q.B. Lin, K.X. Song, B. Liu, H.B. Bafrooei, D. Zhou, W.T. Su, F. Shi, D.W. Wang, H.X. Lin, I. M.Reaney, Vibrational spectroscopy and microwave dielectric properties of $AY_2Si_3O_{10}$ (A = Sr, Ba) ceramics for 5G applications, Ceram. Int. 46 (2020) 1171-1177.

[7] A. Ullah, H. Liu, H. Hao, J. Iqbal, Z. Yao, M. Cao, Influence of TiO_2 additive on sintering temperature and microwave dielectric properties of $Mg_{0.90}Ni_{0.1}SiO_3$ ceramics, J. Eur. Ceram. Soc. 37 (2017) 3045-3049.

[8] X. Zhou, L.T. Liu, J.J. Sun, N.K. Zhang, H.Z. Sun, H.T. Wu, W.H. Tao, Effects of $(Mg_{1/3}Sb_{2/3})^{4+}$ substitution on the structure and microwave dielectric properties of $Ce_2Zr_3(MoO_4)_9$ ceramics, J. Adv. Ceram. 10 (2021) 778-789.

[9] C.Z. Yin, Y. Tang, J.Q. Chen, C.C. Li, L. Fang, F.H. Li, Y.J. Huang, Phase evolution, far-infrared spectra, and ultralow loss microwave dielectric ceramic of $Zn_2Ge_{1+x}O_{4+2x}$ ($-0.1 \leq x \leq 0.2$), J. Mater. Sci.: Mater. Electron. 30 (2019) 16651-16658.

[10] R.D. Shannon, Dielectric polarizabilities of ions in oxides and fluorides, J. Appl. Phys. 73 (1993) 348-366.

[11] R.D. Shannon, G.R. Rossman, Dielectric constants of silicate garnets and the oxide additivity rule, Am. Mineral. 77 (1992) 94-100.

[12] C.Z. Yin, Z.Z. Yu, L.L. Shu, L.J. Liu, Y. Chen, C.C. Li, A low-firing melilite ceramic $Ba_2CuGe_2O_7$ and compositional modulation on microwave dielectric properties through Mg substitution, J. Adv Ceram 10 (2021) 108-119.

[13] X.Q. Song, W.Z. Lu, X.C. Wang, X.H. Wang, G.F. Fan, R. Muhammad, W. Lei, Sintering behaviour and microwave dielectric properties of $BaAl_{2-2x}(ZnSi)_xSi_2O_8$ ceramics, J. Eur. Ceram. Soc. 38 (2018) 1529-1534.

[14] P. Fu, W.Z. Lu, W. Lei, Y. Xu, X.H. Wang, J.M. Wu, Transparent polycrystalline $MgAl_2O_4$ ceramic fabricated by spark plasma sintering: Microwave dielectric and optical properties, Ceram. Int. 39 (2013) 2481-2487.

[15] B. Liu, C.C. Hu, Y.H. Huang, H.B. Bafrooei, K.X. Song, Crystal structure, infrared reflectivity spectra and microwave dielectric properties of $CaAl_2O_4$ ceramics with low permittivity, J. Alloys Compd. 791 (2019) 1033-1037.

[16] Q. Zhang, X.L. Tang, M.F. Zhong, Y.X. Li, Y.L. Jing, H. Su, Bond characteristics and microwave dielectric properties of high-Q materials in li-doped $Zn_3B_2O_6$ systems, J. Am. Ceram. Soc. 104 (2021) 2102-2115.

[17]Y.P. Liu, Y.N. Wang, Y.M. Li, J.J. Bian, Low temperature sintering and microwave dielectric properties of $LiMBO_3$ (M = Ca, Sr) ceramics, Ceram. Int. 42 (2016) 6475-6479.
[18]Z. Xing, C.Z. Yin, Z.Z. Yu, J. Khaliq, C.C. Li, Synthesis of $LiBGeO_4$ using compositional design and its dielectric behaviors at RF and microwave frequencies, Ceram. Int. 46 (2020) 22460-22465.
[19]D. Zhou, L.X. Pang, D.W. Wang, Z.M. Qi, I.M. Reaney, High Quality Factor, Ultralow Sintering Temperature $Li_6B_4O_9$ Microwave dielectric ceramics with ultralow density for antenna substrates, ACS Sustainable Chem. Eng. 6 (2018) 11138-11143.
[20]Y.M. Basalaev, E.S. Boldyreva, E.B. Duginova, Electronic and Vibrational Properties of $LiBO_2$ Crystals, Russ. Phys. J. 61 (2019) 1868-1875.
[21]B.W. Hakki, P.D. Coleman, A dielectric resonator method of measuring inductive capacities in the millimeter range, IRE Trans. Microwave Theory Tech. 8 (1960) 402-410.
[22]I. Kosacki, M. Massot, M. Balkanski, H.L. Tuller, Electrical conductivity and Raman scattering of amorphous V_2O_5-$LiBO_2$, Mater. Sci. Eng. B 12 (1992) 345-349.
[23]A. Rulmont, M. Almou, Vibrational spectra of metaborates with infinite chain structure: $LiBO_2$, CaB_2O_4, SrB_2O_4, Spectrochimica Acta Part A: Molecular Spectroscopy 45 (1989) 603-610.
[24]Y. Xiong, H.Y. Xie, Z.G. Rao, L.J. Liu, Z.F. Wang, C.C. Li, Compositional modulation in $ZnGa_2O_4$ via Zn^{2+}/Ge^{4+} co-doping to simultaneously lower sintering temperature and improve microwave dielectric properties, J. Adv Ceram 10 (2021) 1360-1370.
[25]E.S. Kim, B.S. Chun, K.H. Yoon, Dielectric properties of $[Ca_{1-x}(Li_{1/2}Nd_{1/2})_x]_{1-y}Zn_yTiO_3$ ceramics at microwave frequencies, Mater. Sci. Eng. B 99 (2003) 93-97.
[26]K. Du, F. Wang, X.Q. Song, Y.B. Guo, X.C. Wang, W.Z. Lu, W. Lei, Correlation between crystal structure and dielectric characteristics of Ti^{4+} substituted $CaSnSiO_5$ ceramics, J. Eur. Ceram. Soc. 41 (2021) 2568-2578.
[27]K. Du, X.Q. Song, J. Li, J.M. Wu, W.Z. Lu, X.C. Wang, W. Lei, Optimised phase compositions and improved microwave dielectric properties based on calcium tin silicates, J. Eur. Ceram. Soc. 39 (2019) 340-345.
[28]S.H. Yoon, D. Kim, S. Cho, K.S. Hong, Investigation of the relations between structure and microwave dielectric properties of divalent metal tungstate compounds, J. Eur. Ceram. Soc. 26 (2006) 2051-2054.
[29]Y. Xiong, Z. Xing, J.H. Weng, C. Ma, J. Khaliq, C.C. Li, Low-temperature sintering, dielectric performance, and far-IR reflectivity spectrum of a lightweight NaCaVO4 with good chemical compatibility with silver, Ceram. Int. 47 (2021) 22219-22224.
[30]C.Z. Yin, C.C. Li, G.J. Yang, L. Fang, Y.H. Yuan, L.L. Shu, J. Khaliq, $NaCa_4V_5O_{17}$: A low-firing microwave dielectric ceramic with low permittivity and chemical compatibility with silver for LTCC applications, J. Eur. Ceram. Soc. 40 (2020) 386-390.
[31]E.S. Kim, B.S. Chun, R. Freer, R.J. Cernik, Effects of packing fraction and bond valence on microwave dielectric properties of $A^{2+}B^{6+}O_4$ (A^{2+}: Ca, Pb, Ba; B^{6+}: Mo, W) ceramics, J. Eur. Ceram. Soc. 30 (2010) 1731-1736.
[32]J.Q. Chen, W.S. Fang, L.Y. Ao, Y. Tang, J. Li, L.J. Liu, L. Fang, Structure and chemical bond characteristics of two low-εr microwave dielectric ceramics LiBO2 (B = Ga, In) with opposite τ_f, J. Eur. Ceram. Soc. 41 (2021) 3452-3458.
[33]K. Wakino, M. Murata, H. Tamura, Far Infrared Reflection Spectra of $Ba(Zn,Ta)O_3$-$BaZrO_3$ dielectric resonator material, J. Am. Ceram. Soc. 69 (1986) 34-37.
[34]W.G. Spitzer, R.C. Miller, D.A. Kleinman, L.E. Howarth, Far infrared dielectric dispersion in

$BaTiO_3$, $SrTiO_3$, and TiO_2, Phys. Rev. 126 (1962) 1710-1721.

[35]X.Y. Chen, W.J. Zhang, B. Zalinska, I. Sterianou, S.X. Bai, I.M. Reaney, Low Sintering temperature microwave dielectric ceramics and composites based on Bi_2O_3-B_2O_3, J. Am. Ceram. Soc.95 (2012) 3207-3213.

[36]Y.J. Gu, L.W. Lei, J.L. Huang, X.H. Yang, Q. Li, LH. Li, X.L. Li, B.H. Kim, A novel low-fired, temperature-stable, and low-cost $(1-x)BaCu(B_2O_5)-xTiO_2$ microwave dielectric ceramic, J. Eur. Ceram. Soc. 39 (2019) 1137-1141.

[37]M. Ohashi, H. Ogawa, A. Kan, E. Tanaka, Microwave dielectric properties of low-temperature sintered $Li_3AlB_2O_6$ ceramic, J. Eur. Ceram. Soc. 25 (2005) 2877-2881.

[38]U. Došler, M.M. Kržmanc, D. Suvorov, The synthesis and microwave dielectric properties of $Mg_3B_2O_6$ and $Mg_2B_2O_5$ ceramics, J. Eur. Ceram. Soc. 30 (2010) 413-418.